Establishing Links Between Single Gold Nanoparticles Buried Inside SiO_2 Thin Film and 351-nm Pulsed-Laser-Damage Morphology

Introduction

Over the past several years research has indicated that nanoscale defects, dispersed inside thin films with relatively low abundance, are a major laser-damage-initiation source in the UV spectral range.[1–4] The extreme difficulties in characterizing these defects virtually stalled the experimental effort to identify the laser-damage mechanism. This situation led to a proposed model SiO_2-thin-film system[5] with artificially introduced gold nanoparticles serving as well-characterized absorbing defects.

Advantages of such a system include high intrinsic-damage resistance of SiO_2 thin film—which allows artificially-introduced-defect–driven damage to be separated from the intrinsic damage—and the possibility to control the location and size of the nanoparticles. Optical parameters of gold nanoparticles are well documented in scientific literature,[6] and different-sized particles, with narrow size distributions, are available in the form of gold colloids.

Our previous work[5] focused on comparative atomic force microscopy (AFM) investigation of the nanoparticle and 351-nm damage-crater areal density statistic. The results provided the first experimental evidence of the laser energy absorption process spreading from the defect into the thin-film matrix during the laser pulse. The process starts with an absorption in a particle. As the temperature rises, energy transfer from the particle (via UV radiation, thermionic emission, heat conduction, etc.) to the surrounding matrix causes its effective conversion to an absorptive medium and, consequently, damage.

The next step in this work is to establish a direct link between a single nanoparticle buried inside a SiO_2 thin film at a particular location and the film morphology changes caused by pulsed-laser irradiation. The AFM mapping of the film surfaces after particle deposition and laser-irradiation steps opens the possibility of finding, for each detected damage crater, the corresponding nanoparticle, initiating crater formation. As a result, a key question is addressed—How does the damage scale (crater depth and lateral size) correlate with the particle size? Surprisingly, the correlation appears to be very weak, which is explained by the peculiarities of nanoscale defect/host matrix interaction in the inhomogeneous thin-film medium.

The nanoparticle/damage crater correlations also allow direct comparisons of energy deposited in a particle and energy required for crater formation. The results confirm damage mechanism, considering absorption initiation in a particle with subsequent growth of the absorbing volume within the surrounding film matrix on the later laser-pulse stages.

The same correlations reveal crater formation probabilities as a function of the local laser fluence. By extrapolating a probability curve to zero value, one can find the laser fluence at which only limited matrix melting and no crater formation occur, which, later in this article, will be referred to as "nanoscale" damage threshold. Experimental damage thresholds derived this way allow a more-meaningful comparison with theories that consider matrix melting as a damage onset.

Experimental

1. Damage-Test Sample

   Sample preparation involves several steps:

   (a) Fused-silica glass 7980 is cleaved to ~$14 \times 7 \times 6$-mm pieces to provide a virgin unprocessed surface (14×6 mm) for SiO_2 thin-film deposition.

   (b) The sample is taken to the AFM (Nanoscope III, Digital Inst./Veeco) equipped with a nano-indenting diamond tool, which is used to produce small, ~1-μm-lateral-size, 100-nm-deep indentations organized in a square-type pattern with ~20-μm sides. This pattern is later used as a reference to help find the AFM-mapped areas on the sample surface.

(c) The 120-nm-thick SiO_2 coating is prepared by conventional *e*-beam deposition (base pressure 1.3×10^{-6} Torr; deposition rate 26 nm/min).

(d) Gold nanoparticles in the form of gold colloid are diluted in isopropanol (to achieve an average areal density of 0.3 to 3 μm^{-2}) and deposited by a micropipet onto a SiO_2-coated surface. Three particle sizes are used (5.2-nm, 8.4-nm, and 14.3-nm average diameter) but only one size is used for each experiment. The particle-size distributions provided by the supplier (Ted Pella, Inc.) are presented in Fig. 89.26.

(e) After solvent evaporation (special attention is paid here to the solution-drying protocol to prevent *particle agglomeration*), the sample surface is mapped by the AFM at several locations (each map covers ~6×6-μm area) in the vicinity of the indentations. Only a few agglomerated particles, mostly in the form of duplets, can be found at each location. Their portion is less than 10% of the total particle population.

(f) As a final step, the sample is taken a second time to the coating chamber and coated with an additional 60-nm layer of SiO_2.

The SiO_2 thin-film sample resulting from this procedure is 180 nm thick and contains gold nanoparticles at a well-defined depth of 60 nm (Fig. 89.27).

An additional sample, not containing particles, is prepared for each experiment, following the above protocol, to make available an undoped SiO_2 damage-test reference.

2. Damage Testing and Sample Irradiation Conditions

The 351-nm, 0.5-ns pulses from a Nd-doped glass laser are used for 1-on-1 damage-threshold evaluation. Laser-beam spot size (~400 μm) and fluence distribution are obtained from images captured by a CID (charge-injection device) camera in a sample equivalent plane. Damage onset is detected by means of 110×-magnification dark-field microscopy and, since optical tools are used to determine damage threshold, it will be referred to as an "optical" damage threshold. The "nanoscale" damage threshold, associated with the onset of crater formation and derived from the *AFM investigation* of the post-irradiated coating morphology, will be introduced later in this article. The maximum laser fluence level, used to irradiate the AFM-mapped sites, is varied 10% to 70% above the optical damage threshold. Under these conditions, laser-damage

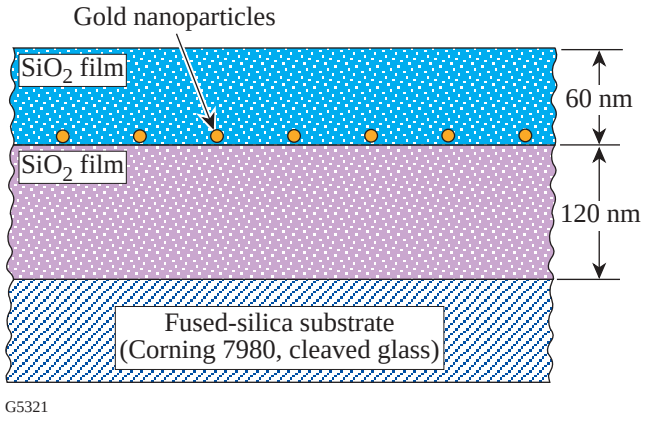

Figure 89.27
Schematic presentation of the SiO_2 sample with embedded gold nanoparticles.

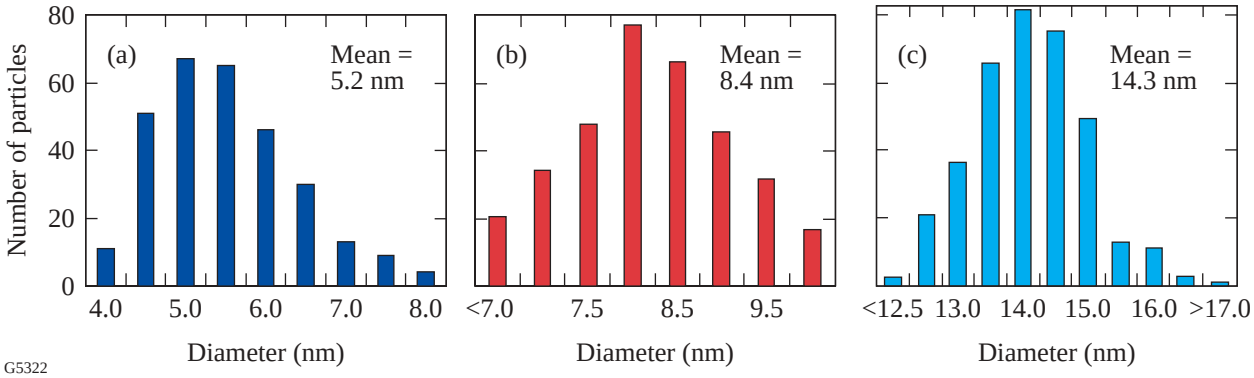

Figure 89.26
Nanoparticle-size distributions provided by the supplier (Ted Pella, Inc.): (a) 5.2-nm, (b) 8.4-nm, and (c) 14.3-nm average diameter.

morphology is represented by submicrometer-scale craters (Fig. 89.28). The laser-beam spot usually covers several mapped sites, which ensures that different damage levels at different mapped sites will be achieved.

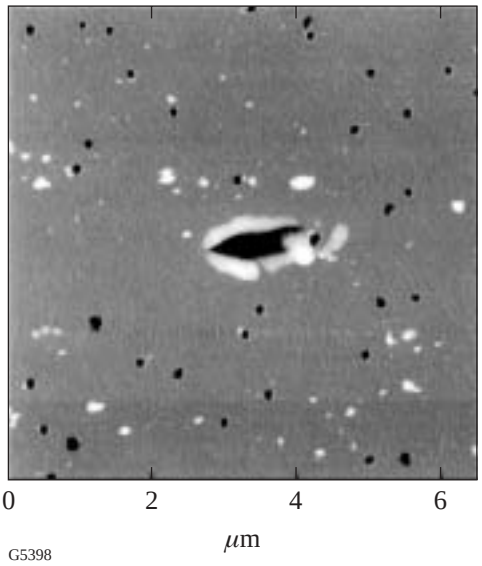

Figure 89.28
The AFM map of a SiO_2 coating containing 8.4-nm gold particles and irradiated by a laser pulse with 4.6-J/cm^2 fluence. The indentation in the center of the map serves as a site identification.

3. AFM Mapping

The very small particle size (up to ~4 nm) limits the maximum AFM scan size during particle mapping. Due to tip-sample convolution effects, a 5-nm-diam particle is typically imaged as a feature with ~20- to 25-nm lateral size. Note that modest convolution does not affect the *vertical* scale, which gives a true particle diameter provided that the pedestal is reasonably flat. Bearing this in mind, 2×2-μm or 3×3-μm AFM scans for 5.2-nm and 8.4-nm particles, correspondingly, were performed. The highest-available, 512×512-pixel image resolution ensures at least five to six data points (pixels) per particle diameter. This requires performing six or seven overlapping, 2×2-μm scans to create a map with a sufficient number of particles for size-effect studies and analyses. The AFM was operated in a tapping mode and employed Si probes with tip radii typically better than 10 nm and apex (last 200 nm) cone angles better than 20°, ensuring ~10-nm lateral resolution. A crater vertical wall slope up to 70° was imaged without convolution along the scan's x axis (along cantilever beam) and up to 80° along the y axis. Typical particle and crater cross-sectional profiles obtained from AFM images are presented in Fig. 89.29.

Results and Discussion

1. Damage Thresholds

The damage-threshold measurement results are summarized in Table 89.I. The introduction of gold nanoparticles causes a dramatic reduction in damage threshold. For the

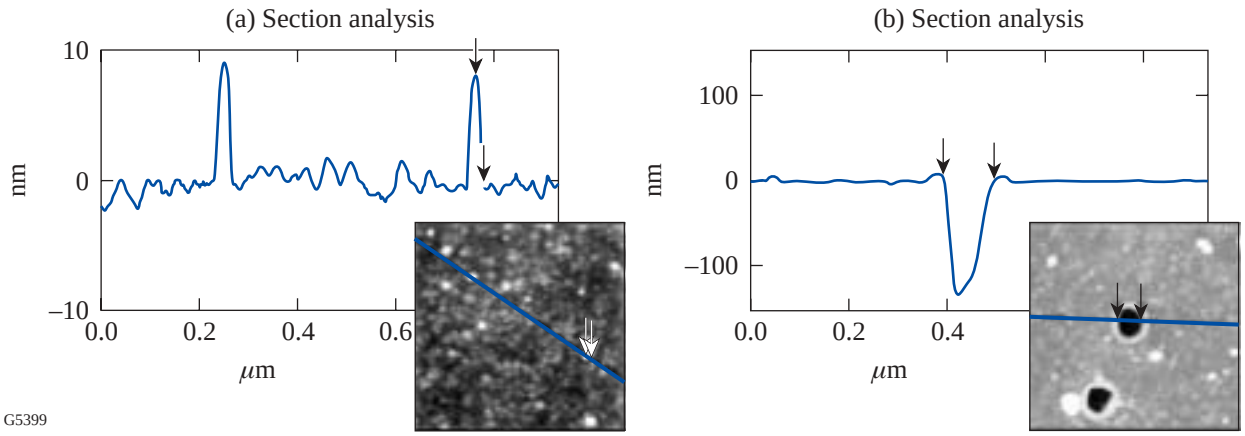

Figure 89.29
Cross-sectional profiles taken through (a) 8.4-nm particles and (b) a typical damage crater.

smallest, 5.2-nm particles, a 4.4-fold reduction, compared to the undoped reference sample, is observed. An even larger threshold drop was found in our previous experiment[5] using the same 5.2-nm particles. It is attributed to particle agglomeration, which is all but eliminated in this work.

The damage-threshold fluence plotted in Fig. 89.30 as a function of the average particle size can be approximated by

$$F_{th} \sim 1/R^t, \quad (1)$$

where R is the particle radius and $t \sim 0.4$ to 1.0.

An extrapolation of this dependence (Fig. 89.30) to the intersection with the threshold value for the undoped reference sample $F_{th} = 27.1$ J/cm^2 allows rough estimates for the absorptivity of the intrinsic absorbing defects. By fitting Eq. (1) to the experimental data with their designated error bars, one finds that the possible range for x intercepts lies between 0.1 nm and 1.4 nm.

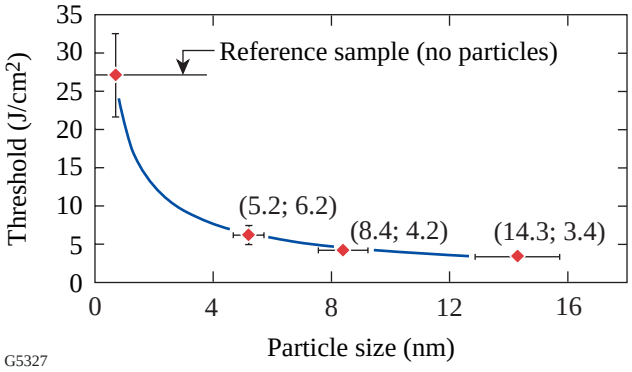

Figure 89.30
Damage threshold as a function of the average particle size. The solid line is the best fit using $F_{th} \sim 1/R^t$ approximation. Numbers in brackets indicate particle size and threshold values, respectively.

It implies that intrinsic defect absorptivity should be similar to the absorptivity of gold particles with a size ≤1.4 nm. Considering Si clusters in SiO_2 film as prime candidates for the intrinsic nanoabsorber role and using Si cluster absorptivity[7] and bandgap/cluster size dependence[8] data, an estimate for the cluster diameter gives values of 1.3 nm ≤ D ≤ 2 nm.

2. Mechanism of Laser-Energy Deposition Inside Thin Film

In all experiments with 5.2-nm and 8.4-nm particles and laser fluences from 2 to 7 J/cm^2, craters were found exclusively at the positions where particles were lodged during deposition (Fig. 89.31). This proves that (1) particles adhere to the SiO_2 film and are not displaced during deposition of the 60-nm capping layer, and (2) absorbing gold defects alone contribute to the damage process at threshold laser fluences.

This one-to-one link between each nanoparticle and the laser-induced local changes in film morphology has a great advantage over other, nonlocal approaches. For instance, energy absorbed by the individual nanoparticle can be compared with energy required to produce a crater at this location. The calculation of energy absorbed by the particle is based on a simple formula:

$$E_{abs} = F\,\sigma_{abs}, \quad (2)$$

where F is the experimentally determined laser-fluence value and σ_{abs} is the Mie[9] absorption cross section.

In the small nanoparticle approximation $2R << \lambda$, fully applicable for particle sizes used in this work, according to the Mie theory,[9] the cross section of this process is dominated by dipolar absorption:

$$\sigma_{abs}(\omega) = 9\frac{\omega}{c}\varepsilon_m^{3/2}V_0\frac{\varepsilon_2(\omega)}{\left[\varepsilon_1(\omega)+2\varepsilon_m\right]^2+\varepsilon_2(\omega)^2}, \quad (3)$$

Table 89.I: Damage thresholds of SiO_2 film containing gold nanoparticles.

Nanoparticle Average Size (nm)	Damage Threshold (J/cm^2)
5.2	6.2±0.2
8.4	4.2±0.1
14.3	3.4±0.2
Reference sample (no particles)	27.1±3.0

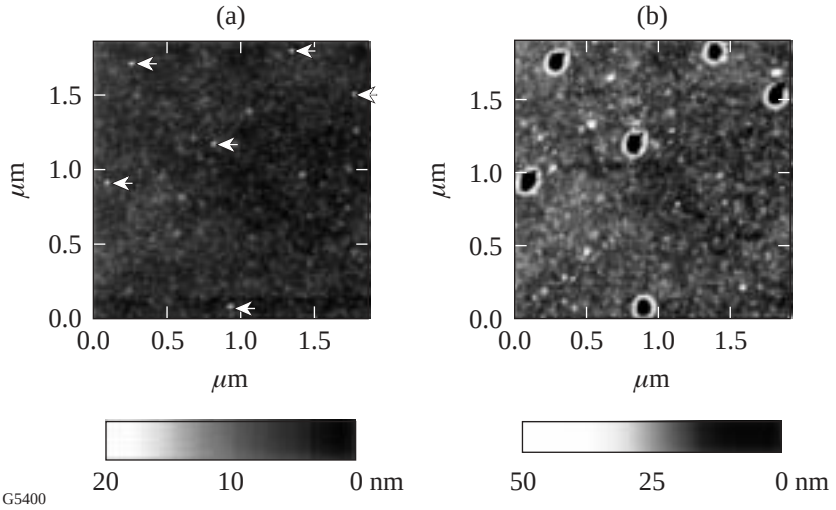

Figure 89.31
AFM images of ~2 × 2-μm surface area containing six nanoparticles: (a) nanoparticle map, (b) same area after 60-nm SiO_2 overcoat and irradiation. The craters are formed at exactly the nanoparticle locations.

where V_0 is the particle volume [$V_0 = (4/3)\,\pi R^3$], ε_m is the dielectric function of the medium (SiO_2), $\varepsilon_1(\omega)$ and $\varepsilon_2(\omega)$ are the real and imaginary parts, respectively, of the particle dielectric function, and ω is the laser frequency. The calculation was done for particle sizes ranging from 4 nm to 12 nm, $\varepsilon_m = 2.19$ for SiO_2, and data for ε_1 and ε_2 are taken from Kreibig *et al.*[6]

The energy required to produce a crater can be estimated by assuming that the material within the crater volume is heated up to the boiling point with subsequent vaporization. The presence of the melting stage is supported by the crater morphology. The glassy, structureless walls and a rim elevated above average surface level [Fig. 89.29(b)] are missing the characteristic granular structure of the surrounding film, which provides clear evidence for melting and resolidification into the glass-type structure during the cooling stage.

Assuming this mechanism, the energy required for crater formation is expressed as

$$E_{\mathrm{cr}} = V_{\mathrm{cr}}\left[C\rho\left(T_b - 293\,\mathrm{K}\right) + H_{\mathrm{fus}} + H_{\mathrm{vap}}\right], \qquad (4)$$

where V_{cr} is the crater volume, C is the silica heat capacity, ρ is the density, T_b is the boiling point, and H_{fus} and H_{vap} are the heat of fusion and heat of vaporization, respectively. Values of the parameters used for the calculation of E_{cr} are $C = 741$ J/kg K, $\rho = 2200$ kg/m^3, $T_b = 2503$ K, $H_{\mathrm{fus}} = 3.12 \times 10^8$ J/m^3, and $H_{\mathrm{vap}} = 7.6 \times 10^9$ J/m^3.

C and ρ are considered independent of temperature for a lack of available high-temperature data (>2000 K). Taking into account that the heat capacity for most glasses increases over the temperature interval of 1 K to 1900 K would result in an ~16% increase in the E_{cr} value calculated from Eq. (4). V_{cr} is derived from AFM data.

The results of calculations for E_{abs} and E_{cr} for eight selected nanoparticles and corresponding craters are presented in Table 89.II, which clearly shows that, considering that the energy absorption process is localized inside the particle, the amount of energy absorbed cannot provide crater formation since $E_{\mathrm{abs}} < E_{\mathrm{cr}}$ for all but one particle (last row).

This conclusion is valid not only for a chosen set of particles and corresponding craters but also for the majority of such pairs from Fig. 89.32 and all particle/crater pairs from Figs. 89.33(b) and 89.33(c). One must also keep in mind that the energy balance considerations, presented above, are simplified. It implies that all of the energy absorbed inside the particle is used to form a crater. It does not take into account the heating of the volume surrounding the crater and particle, as well as radiative losses. The former contribution can be quite significant since the temperatures in the immediate particle vicinity are much higher than at the sample surface.

These additional dissipation channels cause the energy deficit between E_{abs} and E_{cr} to widen, confirming earlier[5] findings that *absorption initiated in the gold nanoparticle spreads out to the surrounding matrix during the laser pulse*. The conversion of the transparent matrix into an absorptive medium involves energy transfer from the particle heated to a high (up to ~10^4 K) temperature.[10] The possible channels include ionization by thermal UV radiation,[10] electron injection through thermionic emission, and thermal ionization via

conductive heat transfer.[11] The modeling of absorbing volume (plasma ball) growth by Feit *at al.*[12] pointed to exponential behavior of this process as a function of laser fluence.

3. Nanoparticle Size/Damage-Crater-Depth Correlations

The next question to be addressed is how damage-crater scale (depth, lateral size) correlates with particle size. Since the crater's lateral size and depth showed qualitatively similar behavior as a function of particle size, the crater depth is used here for illustration purposes. It is useful to mention here that the intuitive expectation that the crater depth should be the well-defined depth (60 nm) at which particles are lodged is not supported by the experimental results. In fact, craters with depths ranging from 10 to 160 nm are produced for 5.2-nm- and 8.4-nm-average-size particles at different laser fluences (see Figs. 89.32 and 89.33). If energy deposited in the absorbing volume is low, only partial evaporation of the material above the particle takes place and shallow craters with depths <<60 nm are formed. In the other limit, with increasing energy, the absorbing volume is also growing and craters with depths exceeding 60 nm can be formed. In the first approximation [Eq. (3)], the absorption cross section for small particles is proportional to the particle volume V_0. Accordingly, one might expect fairly strong crater-size/particle-size dependence. Experimental findings showed two distinctively different cases, represented in Figs. 89.32 and 89.33.

Table 89.II: Energy absorbed by the particle and energy required for crater formation.

Particle Size (nm)	σ_{abs} (cm^2)	F (J/cm^2)	E_{abs} (J)	Crater		
				Depth (nm)	Lateral Size* (nm)	E_{cr} (J)
4.0	2.2×10^{-14}	3.2	7.0×10^{-14}	60	47	4.0×10^{-13}
5.3	4.9×10^{-14}	4.0	2.0×10^{-13}	72	53	6.1×10^{-13}
6.3	7.1×10^{-14}	4.0	2.8×10^{-13}	86	64	1.1×10^{-12}
8.1	1.7×10^{-13}	4.0	6.8×10^{-13}	88	63	1.1×10^{-12}
9.2	2.5×10^{-13}	4.6	1.2×10^{-12}	120	83	2.5×10^{-12}
10.4	3.4×10^{-13}	4.6	1.6×10^{-12}	124	95	3.4×10^{-12}
11.8	5.2×10^{-13}	4.6	2.4×10^{-12}	130	112	4.9×10^{-12}
10.0	3.2×10^{-13}	2.3	7.4×10^{-13}	54	50	4.1×10^{-13}

*The lateral size is measured at the average level of the film surface [see Fig. 89.29(b)].

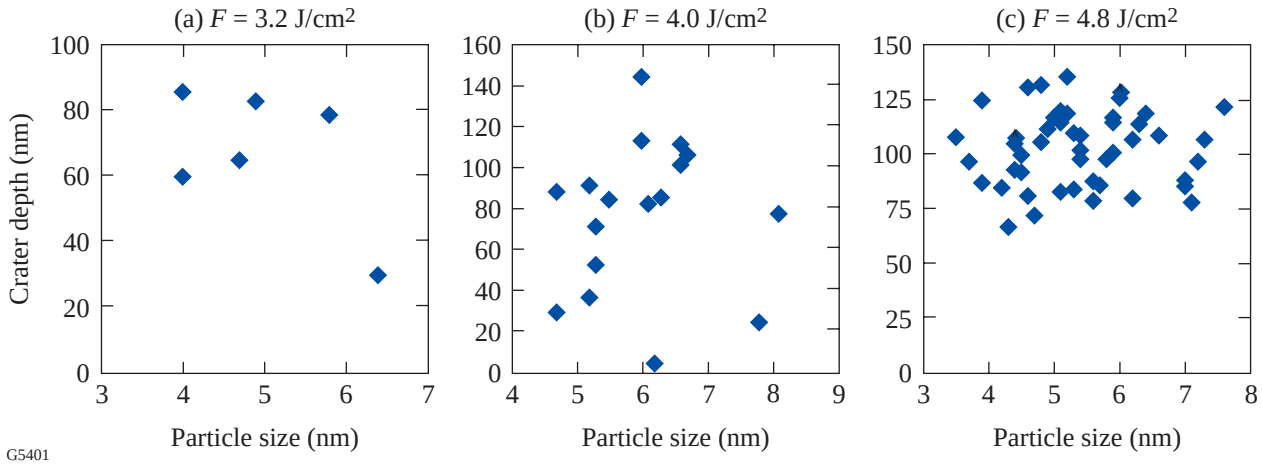

Figure 89.32
Crater depth as a function of the particle size for 5.2-nm-average-size particles and laser fluence (a) 3.2 J/cm^2, (b) 4.0 J/cm^2, and (c) 4.8 J/cm^2.

In the first case, described by laser fluences of less than 70% of the optical damage threshold, almost *no correlation* is found between particle size and crater depth [Figs. 89.32(a), 89.32(b), and 89.33(a)]. Moreover, at these low laser fluences, when a minor fraction of particles gives rise to crater formation, a situation is frequently encountered where small particles form craters but a larger particle located within a distance of ~1 μm does not. At a constant laser fluence for both particles, the strong influence of the inhomogeneous local particle environment inside the SiO_2 film becomes apparent for the laser-energy absorption process and the dissipation channels.

In agreement with a model that considers the effective growth of the absorbing volume caused by particle/matrix interaction during the laser pulse, two factors define the effectiveness of laser-energy deposition:

a. Absorption of laser-pulse energy by the particle itself. In a porous thin-film medium, the nanoparticle's physical contact with the host matrix is not perfect (Fig. 89.34), which results in the effective dielectric function ε_{eff}:

$$\varepsilon_m \geq \varepsilon_{\text{eff}} \geq \varepsilon_{\text{air}} = 1. \quad (5)$$

Taking data from the literature[6] on ε_i (351 nm) for nanoparticles with size $2R$ = 5 nm ($\varepsilon_1 = -0.8$, $\varepsilon_2 = 6.2$) and ε_m (SiO_2) = 2.19, we obtain from Eq. (3)

$$\sigma_{\text{abs}}(\text{SiO}_2)/\sigma_{\text{abs}}(\text{air}) = 2.5.$$

This result reveals the potential for significant variation in the effectiveness of damage initiation depending on the local physical environment of each gold nanoparticle.

b. Absorption by the matrix modified via energy transfer from the heated particle. Energy transfer from a particle heated to a high temperature in the early stages of the laser pulse to the surrounding film matrix is an essential part of the damage process. To achieve absorption in the particle-surrounding matrix, the energy should be transferred in a time scale of laser pulse length. Any air voids between particle and matrix (Fig. 89.34) will dramatically reduce the rate of such processes as either heat transfer by thermal conductivity or injection of electrons through thermionic emission. The same voids of the order of particle radius, due to geometrical factor, will reduce fluence of the UV radiation coming from the heated particle and consequently matrix ionization rate.

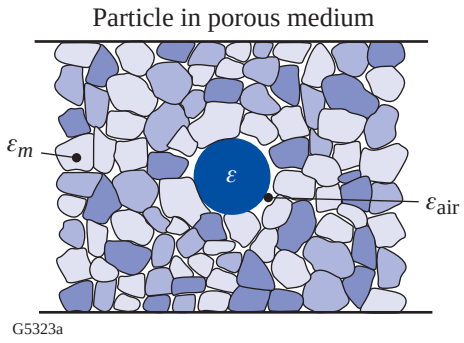

Figure 89.34
Schematic presentation of the particle embedded in the porous medium.

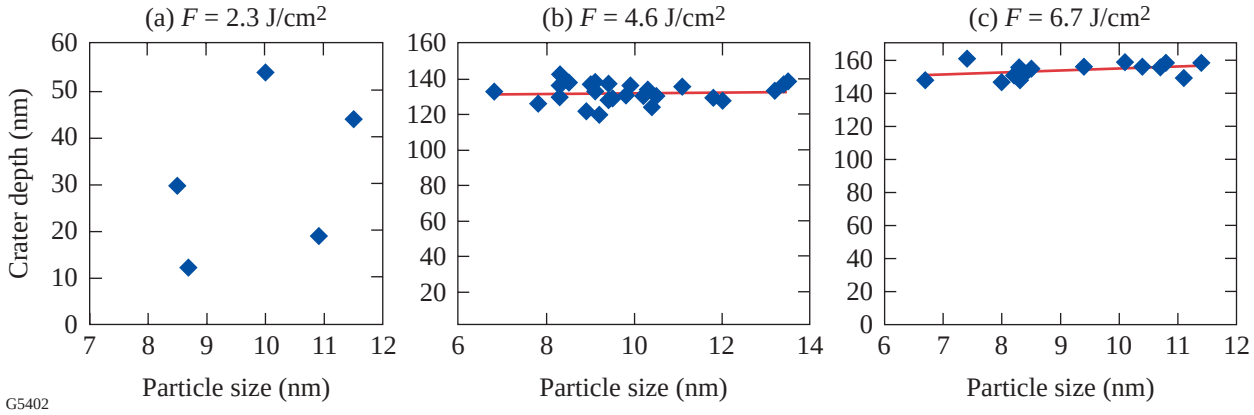

Figure 89.33
Crater depth as a function of the particle size for 8.4-nm-average-size particles and laser fluence (a) 2.3 J/cm^2, (b) 4.6 J/cm^2, and (c) 6.7 J/cm^2.

As a conclusion, effectiveness of the energy transfer from the particle to the surrounding matrix, facilitating growth of the absorbing volume and energy acquisition from the laser pulse, is a strong function of the local particle environment.

In summary, randomness in the local particle environment in the inhomogeneous thin-film medium introduces random variations in crater size and the probability of crater formation. These variations, at laser fluences below optical damage threshold, dominate particle-size effects as long as the size variation is modest, i.e., ±25%. An interesting implication from the above considerations is that porous thin films with large voids might be more damage resistant than dense films, provided that nanoscale absorbers remain the same. High UV damage thresholds of sol-gel–derived coatings,[13] characterized by large free volume, provide additional support for such a hypothesis.

The second case is characterized by very slow linear behavior of crater-depth/particle-size dependence at laser fluences *exceeding* the threshold by 20% to 70% [Figs. 89.33(b) and 89.33(c)]. At these laser-fluence conditions, all gold nanoparticles, mapped by the AFM, give rise to crater formation (100% probability), yet craters show surprisingly narrow depth distributions. Such a trend provides an indication that, with increasing pulse energy, the influence of initial conditions (local environment; particle-size variation) on the final result—crater formation—becomes less important. This can be explained by assuming that the ionized matrix in the particle vicinity starts taking on the dominant absorber role. In this case, the effective absorbing volume of the matrix should be much larger than the particle volume. The radius of this matrix volume should be several times larger than both the particle radius and the average void diameter. Such an increase in effective absorbing volume allows averaging over many local inhomogeneities, resulting in a significant reduction in random variation of the crater depth.

An example of the intermediate case for 5.2-nm particles is presented in Fig. 89.32(c), where crater-depth variation is reduced compared to the low fluence data in Figs. 89.32(a) and 89.32(b), but still significantly larger than for the above-threshold fluence data presented in Figs. 89.33(b) and 89.33(c).

To summarize results on particle/crater correlations: At laser fluences below the optical-damage threshold, effects caused by ±25% variations in particle size are obscured by strong local influence of the inhomogeneous thin-film medium on the crater-formation process. With increasing laser fluence, the probability of crater formation also increases, while the crater-depth variation is reduced due to the averaging effect caused by the larger absorption volume.

4. Crater-Formation Probability and "Nanoscale" Damage Thresholds

The possibility of detecting laser-induced morphological changes in thin film at each mapped nanoparticle location allows one to investigate the probability of crater formation for an ensemble of particles confined to a small area (typically ~6 × 6 μm), within which the laser fluence can be considered constant.

The probability of crater formation can be defined as the ratio of the number of particles giving rise to crater formation to the total number of particles within the mapped area. Taking into account that craters are detected only at particle locations, this is also the ratio of the number of craters to the total number of particles within the area. The probabilities calculated in this way for 5.2-nm- and 8.4-nm-average-diam particles are presented in Fig. 89.35 as a function of laser fluence. An extrapolation of the crater- formation probability curve to zero probability level allows one to define a laser-fluence value at which only localized melting and no vaporization of the material are observed.

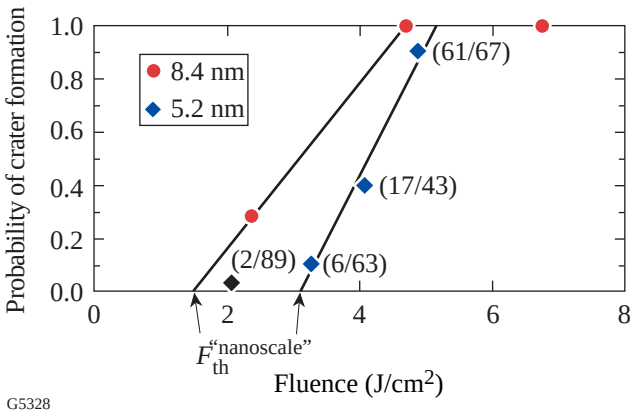

Figure 89.35
Probability of crater formation as a function of laser fluence. Numbers in brackets indicate crater/particle ratio for each mapped site. Nanoscale damage thresholds are derived from an extrapolation to zero probability.

Defined this way, *nanoscale* damage thresholds are derived as ~3.0 J/cm^2 and ~1.5 J/cm^2 for 5.2-nm and 8.4-nm particles, respectively. These are more than a factor of 2 lower than the ones obtained through optical microscopy observation. The introduction of such a threshold establishes a basis for more-meaningful comparison between theory and experiment, since

the majority of theoretical approaches consider damage onset to occur when the film material reaches the melting temperature.

Recent theoretical work by P. Grua and H. Bercegol[14] applied the Mie theory to a similar system of gold nanoparticles embedded in a glass matrix. The gold particle reaching the melting temperature was chosen as a damage criterion for calculating damage threshold. For 3.6-eV photon energy (photon energy of 351-nm radiation = 3.53 eV), 0.5-ns pulses, and particles of $2R$ = 6-nm size, the calculated damage threshold becomes ~0.4 J/cm^2. This value is much lower than ~3-J/cm^2 nanoscale threshold for 5.2-nm-average-size particles obtained in this work and associated with the matrix melting. The difference may be attributed partially to the fact that gold's melting temperature T_{Au} = 1336 K is much lower than silica's melting temperature T_{SiO_2} = 1986 K, which again points to the importance of using similar damage criteria for both theory and experiment. In the work of F. Bonneau *et al*.,[15] the simulations of nanometer-scale-inclusion–driven laser damage of fused silica indicated that damage onset occurred when the SiO_2 matrix reached the melting point. For 10-nm-diam Al nanoparticles and irradiation conditions identical to this work (351 nm, 0.5 ns), the calculated threshold was $F_{th} \sim 2$ J/cm^2. The fact that this article reports nanoscale threshold of 1.5 J/cm^2 for similar-sized, 8.4-nm gold particles unfortunately does not indicate an agreement between theory and experiment. Taking into account the difference in the absorption cross section and other relevant parameters for aluminum and gold results in a significant reduction in the calculated threshold value when substituting Al particles with Au. This points to the necessity for further theoretical and experimental investigation of the damage mechanisms.

Conclusions

- Introduction of gold nanoparticles into an SiO_2 thin film leads to a significant reduction in 351-nm damage thresholds. An extrapolation of damage threshold versus particle size curve to the intersection with undoped sample threshold allows one to estimate the size of intrinsic nanoscale absorbers (presumably Si clusters) as 1.3 to 2 nm.

- AFM mapping shows excellent correspondence between particle and crater location, indicating that absorption by gold particles is solely responsible for the damage initiation.

- Numerical estimates of energy absorbed by gold particles and energy required to melt and evaporate material within the crater volume confirm that laser-energy absorption cannot be confined inside the particle, but rather starts in the particle and then, upon temperature rise, spreads out to the surrounding matrix.

- The particle/crater correlations show peculiarities that can be explained by the influence of thin-film inhomogeneities. At laser fluences below damage threshold, the probability of crater formation and damage extent (crater depth) strongly depends on the local particle environment—effective dielectric constant, void geometry, etc. When laser fluence exceeds the optical damage threshold, the crater-depth/particle-size dependence approaches very slow linear behavior. This is explained by the dominating role of absorption by the defect-surrounding matrix, the volume of which is much larger than both the volume of the particle and characteristic film inhomogeneity.

- The observed strong influence of the thin-film structure on UV-damage initiation indicates that thin-film damage resistance can benefit from higher film porosity.

- Crater formation probability as a function of laser fluence allows one to define conditions when absorption by the particle is causing only limited melting in the surrounding matrix without significant vaporization (crater formation). A laser fluence corresponding to these conditions is introduced as a nanoscale damage threshold, which should facilitate a more-meaningful comparison with theoretical predictions using the onset of the matrix melting as a damage benchmark.

ACKNOWLEDGMENT

This work was supported by the U.S. Department of Energy Office of Inertial Confinement Fusion under Cooperative Agreement No. DE-FC03-92SF19460, the University of Rochester, and the New York State Energy Research and Development Authority. The support of DOE does not constitute an endorsement by DOE of the views expressed in this article.

REFERENCES

1. S. Papernov, A. W. Schmid, J. Anzelotti, D. Smith, and Z. R. Chrzan, in *Laser-Induced Damage in Optical Materials: 1995*, edited by H. E. Bennett *et al.* (SPIE, Bellingham, WA, 1996), Vol. 2714, pp. 384–392.

2. J. Dijon *et al.*, in *Laser-Induced Damage in Optical Materials: 1995*, edited by H. E. Bennett *et al.* (SPIE, Bellingham, WA, 1996), Vol. 2714, pp. 416–419.

3. J. Dijon, T. Poiroux, and C. Desrumaux, in *Laser-Induced Damage in Optical Materials: 1996*, edited by H. E. Bennett *et al.* (SPIE, Bellingham, WA, 1996), Vol. 2966, pp. 315–325.

4. S. Papernov and A. W. Schmid, J. Appl. Phys. **82**, 5422 (1997).

5. S. Papernov, A. W. Schmid, R. Krishnan, and L. Tsybeskov, in *Laser-Induced Damage in Optical Materials: 2000*, edited by G. J. Exarhos *et al.* (SPIE, Bellingham, WA, 2001), Vol. 4347, pp. 146–154.

6. U. Kreibig and M. Vollmer, *Optical Properties of Metal Clusters*, Springer Series in Materials Science, Vol. 25 (Springer-Verlag, Berlin, 1995).

7. K. Kohno *et al.*, Jpn. J. Appl. Phys. 1, Regul. Pap. Short Notes **33**, 6616 (1994).

8. L. Patrone *et al.*, J. Appl. Phys. **87**, 3829 (2000).

9. G. Mie, Ann. Phys. **25**, 377 (1908); C. F. Bohren and D. R. Huffman, *Absorption and Scattering of Light by Small Particles* (Wiley, New York, 1983).

10. Yu. K. Danileiko, A. A. Manenkov, and V. S. Nechitailo, Sov. J. Quantum Electron. **8**, 116 (1978).

11. L. B. Glebov, in *Laser-Induced Damage in Optical Materials: 2000*, edited by G. J. Exarhos *et al.* (SPIE, Bellingham, WA, 2001), Vol. 4347, pp. 343–358.

12. M. D. Feit *et al.*, in *Laser-Induced Damage in Optical Materials: 1997*, edited by G. J. Exarhos *et al.* (SPIE, Bellingham, WA, 1998), Vol. 3244, pp. 350–355.

13. H. A. McInnes *et al.*, in *Laser-Induced Damage in Optical Materials: 2000*, edited by G. J. Exarhos *et al.* (SPIE, Bellingham, WA, 2001), Vol. 4347, pp. 118–126.

14. P. Grua and H. Bercegol, in *Laser-Induced Damage in Optical Materials: 2000*, edited by G. J. Exarhos *et al.* (SPIE, Bellingham, WA, 2001), Vol. 4347, pp. 579–587.

15. F. Bonneau *et al.*, in *Laser-Induced Damage in Optical Materials: 2000*, edited by G. J. Exarhos *et al.* (SPIE, Bellingham, WA, 2001), Vol. 4347, pp. 308–315.